Nanoscale Research Letters
a SpringerOpen Journal

NANO EXPRESS Open Access

The electronic structure and optical properties of Mn and B, C, N co-doped MoS_2 monolayers

Wei-bin Xu, Bao-jun Huang, Ping Li, Feng Li, Chang-wen Zhang and Pei-ji Wang*

Abstract

The electronic structure and optical properties of Mn and B, C, N co-doped molybdenum disulfide (MoS_2) monolayers have been investigated through first-principles calculations. It is shown that the MoS_2 monolayer reflects magnetism with a magnetic moment of 0.87 μB when co-doped with Mn-C. However, the systems co-doped with Mn-B and Mn-N atoms exhibit semiconducting behavior and their energy bandgaps are 1.03 and 0.81 eV, respectively. The bandgaps of the co-doped systems are smaller than those of the corresponding pristine forms, due to effective charge compensation between Mn and B (N) atoms. The optical properties of Mn-B (C, N) co-doped systems all reflect the redshift phenomenon. The absorption edge of the pure molybdenum disulfide monolayer is 0.8 eV, while the absorption edges of the Mn-B, Mn-C, and Mn-N co-doped systems become 0.45, 0.5, and 0 eV, respectively. As a potential material, MoS_2 is widely used in many fields such as the production of optoelectronic devices, military devices, and civil devices.

Keywords: MoS_2 monolayer; Mn-B co-doped; Mn-C co-doped; Mn-N co-doped; Electronic structure; Optical properties

Background

Layered transition metal dichalcogenides (TMD) belong to a well-defined chemical and structural family characterized by strong covalent intralayer bonding and weak van der Waals interactions between adjacent layers [1,2]. Transition metal oxides and sulfides have always been an interesting subject in experimental and theoretical works [3-9] due to their important role in lithium-ion batteries (LIB) [10], flexible electronic devices [11], photoluminescence [12], valleytronics [13,14], and field-effect transistors. Molybdenum disulfide (MoS_2) monolayer contains hexagonal planes of Mo atoms lying between two hexagonal planes of S atoms, forming a sheet of S-Mo-S. Each Mo atom bonds with six neighboring S atoms through covalent bonds.

Cheng et al. [15] have found that the formation energy of substitutional doping is formidably large in graphene, rendering doping in this 2D material a challenging issue. It has been proved that a very thin MoS_2 owns a good property of lubrication. It is mainly because the binding energy between S atoms and metal materials is so strong that MoS_2 has a great adsorbability on the metal surface. MoS_2 can also be used as a kind of desulfurization catalyst [16,17] for crude oil in the industry, indeed preventing the phenomenon of sulfur poisoning. Due to its good chemical stability, thermal stability, specific surface area, and high surface activity, MoS_2 can be a utility material. Though its optical and electronic properties [18-24] have been discussed, MoS_2 still has limitations in improving the optical property for the production of photodetectors in the industry. Doping in MoS_2 [25-27], as a typical 2D material, attracts more attention. Through a series of calculations, Mn doping and B (C, N) doping can improve the characters of MoS_2 [24,25]. In order to get more ideal characters of MoS_2, we calculated three structures including Mn-B, Mn-C, and Mn-N co-doped MoS_2 monolayers in this paper. The MoS_2 monolayer co-doped with Mn-C reflects magnetism. However, the systems co-doped with Mn and B (N) atoms exhibit semiconducting behavior with bandgaps smaller than those of the corresponding primitive state. Mn-B (C, N) co-doping all make the optical absorption edges generate the redshift phenomenon for the MoS_2 monolayer, which results in the enhancement of absorption for infrared light in the MoS_2 monolayer. The redshift degree of the Mn-N co-doped system is the largest. This result may open a new route to MoS_2 in optical device applications.

* Correspondence: ss_wangpj@ujn.edu.cn
School of Physics and Technology, University of Jinan, Nan Xin Zhuang west road No. 336, Jinan, Shandong 250022, People's Republic of China

Methods

In this paper, we will discuss three co-doped structures: Mn-B, Mn-C, and Mn-N co-doped MoS_2 monolayers, as shown in Figure 1. All of the computations are performed using the spin-polarized density functional theory with an all-electron linearized augmented plane wave method, as implemented in the WIEN2K simulation package [28], in order to investigate the electronic and optical properties of the MoS_2 monolayer. The cutoff energy is 300 eV, and the muffin tin radius of Mo, S, Mn, B, C, and N is 1.45, 1.04, 1.40, 0.85, 0.70, and 0.65 Å, respectively. A generalized gradient approximation [29] is used to treat the exchange correlation potential, and relativistic effects are taken into account. In order to get comprehensive results about the Mn-3d orbit, the GGA + U method is also used. The $4 \times 4 \times 1$ supercell of MoS_2 with $a = b$ =12.66 Å [30,31] is adopted through all the calculations, and the 2D MoS_2 are located in the x-y plane with periodic boundary conditions and are modeled in a supercell with a vacuum space of at least 20 Å in the z-axis in order to avoid interactions between adjacent sheets. The Brillouin zone (BZ) is represented by a set of $6 \times 6 \times 1$ k-points [32] for geometry optimization and for static total energy calculations. Structural relaxation is done until the forces on each atom are smaller than 10^{-2} eV/Å.

Results and discussion

Formation energy and crystal structure

The relative stability of the doped structure is determined from the formation energy and relates to the realization in experiments. Through co-doping, the formation energy can be calculated by the following general equation, which is inferred from some experiences of other semiconductor materials in any form [33-36]:

$$E_{\text{form}} = E_{\text{tot}}[X] - E_{\text{tot}}[\text{MoS}_2] - \sum n_i E_i$$

$E_{\text{tot}}[\text{MoS}_2]$ and $E_{\text{tot}}[X]$ represent the total energy of the primitive MoS_2 monolayer and the total energy doped with impurities, respectively. $n_i > 0$ means the number of atoms which are doped into the system, while $n_i < 0$ means the number of atoms which are replaced from the MoS_2 monolayer. E_i represents the energy of the single atom. The smaller the value of the formation energy, the greater the stability of the structure. The formation energy under the circumstances of Mn and B, C, N co-doped MoS_2 monolayers is 7.42, 7.03, and 7.56 eV, respectively. Obviously, the case of the Mn-C co-doped system obtains the most stable state.

Due to the sandwich structure of MoS_2, we put our point to the buckled height between two S atom planes (h), the length of Mo-S (d), and the S-Mo-S bond angle (θ) which are 3.16 Å, 2.42 Å, and 81.65°, respectively. As is known,

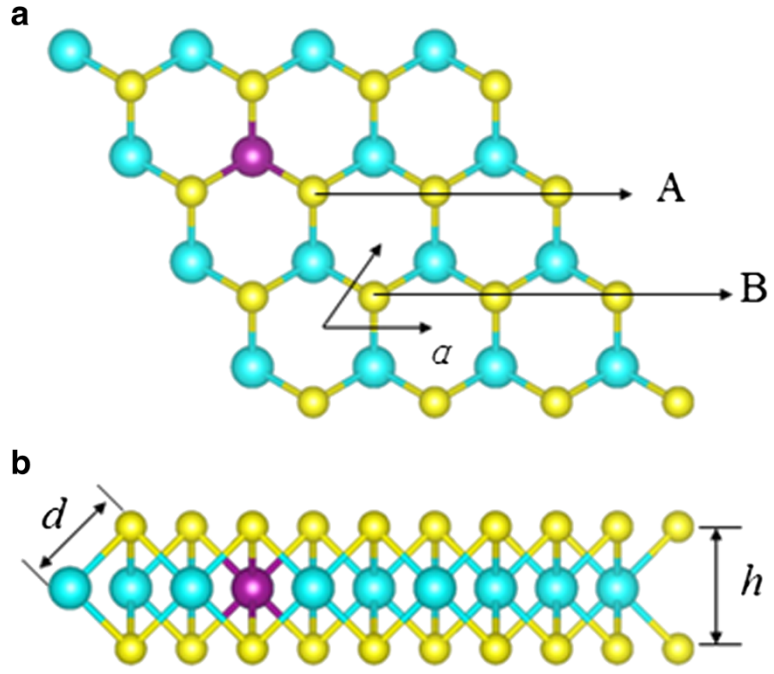

Figure 1 Optimized geometric structures of the MoS_2 monolayer from the top view (a) and side view (b). The blue, yellow, and purple balls are Mo, S, and Mn atoms, respectively. B or C atom substitutes for the S atom at site A, and N atom replaces the S atom located at site B.

Table 1 The crystal structure of the co-doped MoS_2 monolayers

	h (S-S)	*θ* (S-Mo-S)	*d* (Mn-S)	*d* (Mn-*X*)	*d* (Mo-*X*)
Mn-B	3.15	81.88	2.29	2.01	2.12
Mn-C	3.14	81.44	2.32	1.93	2.05
Mn-N	3.14	81.34	2.33	4.95	1.99

The symbols *h*, *d*, and *θ* are the buckled height, bond length, and bond angle, respectively (*X* = B, C, N).

the order of radius for nonmetallic atoms is N > C > B. Table 1 shows us that, with the increase of the radius, *θ* (S-Mo-S) becomes smaller and also the bond length between Mn and S becomes longer and *d* (Mo-*X*) becomes shorter. The buckled height *h* (S-S) under the circumstance of co-doping is smaller than that of the primitive state.

Density of states

In Figure 2, we further present the total density of states (DOS) of all structures. Although the pure MoS_2 monolayer is a nonmagnetic semiconductor, the Mn doping results in magnetic states with spin-up and spin-down branches being unequally occupied. The result well agrees with ref. [26]. From DOS, $Mo_{15}MnCS_{31}$ becomes a magnetic semiconductor, which spins up and spins down asymmetrically. Mostly in view of the orbital coupling between C-2 s, C-2p and Mn-3d, Mn-4 s, Mo-5 s, a series of local energy levels appear around the Fermi level.

However, both $Mo_{15}MnBS_{31}$ and $Mo_{15}MnNS_{31}$ are still semiconductors, which spin up and spin down symmetrically. In $Mo_{15}MnCS_{31}$, the role of Mn upon the conduction band is stronger than that in $Mo_{15}MnS_{32}$. This phenomenon is due to the Mn and C atoms sharing pairs of electrons. Meanwhile, the interaction between electric charges is reinforced and the polarization phenomenon generated. Consequently, the role of Mn-3d upon the conduction band around the Fermi level is reinforced.

To better understand the effect between different orbits, we demonstrate the partial density of states as shown in Figure 3. In $Mo_{15}MnBS_{31}$, the top of the valence band is contributed by B-2p and the bottom of the conduction band is determined by Mn-4 s and B-2p in the majority. Between −3 and −2.5 eV, the valence band is mainly determined by B-2 s and S-3p. The role of B-2 s upon the conduction band between 1.5 and 3 eV is more important than that of B-2p. When the MoS_2 monolayer is co-doped with Mn-C, several local energy levels appear around the Fermi level. This phenomenon is mostly due to the orbital coupling between C-2 s, C-2p and Mn-3d, Mn-4 s. In $Mo_{15}MnNS_{31}$, the top of the valence band as well as the bottom of the conduction band is mainly contributed by N-2 s and Mn-4 s, respectively. N-2 s plays an important role between −0.4 and −0.1 eV in the valence band.

In order to realize the effect of the Mn-3d orbit deeply, the GGA + U method is used. The results show us that the orbital coupling between C-2 s, C-2p and Mn-3d becomes stronger as *U* increases. And the electronic transition between B-2p, C-2 s, C-2p, N-2 s and Mn-3d becomes more active. Above all, the role of Mn-3d enhanced. Considering the Coulomb repulsion between the electrons, the results become convincing.

Energy bandgap

The primitive MoS_2 monolayer has a direct bandgap of 1.85 eV which is consistent with ref. [3]. The band

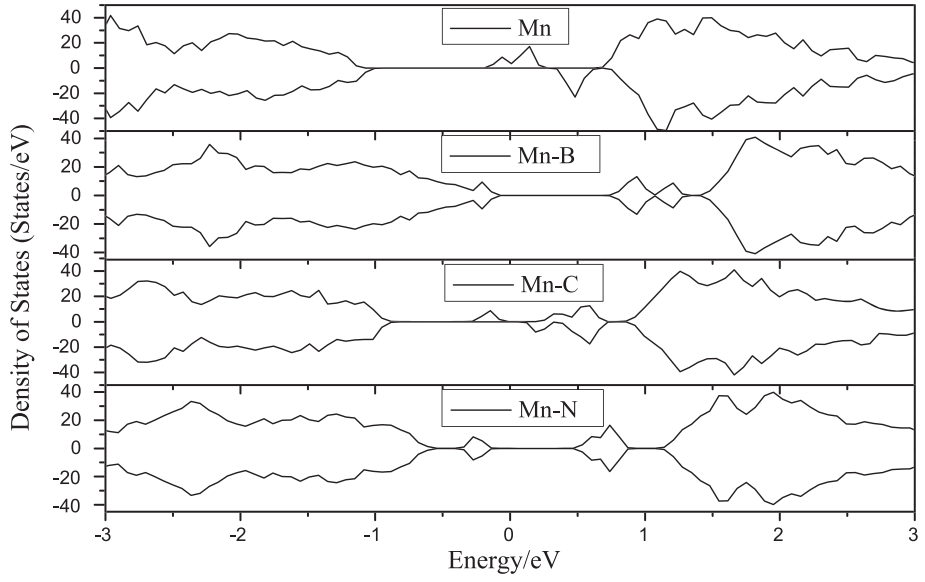

Figure 2 Total density of states of $Mo_{15}MnBS_{31}$, $Mo_{15}MnCS_{31}$, and $Mo_{15}MnNS_{31}$.

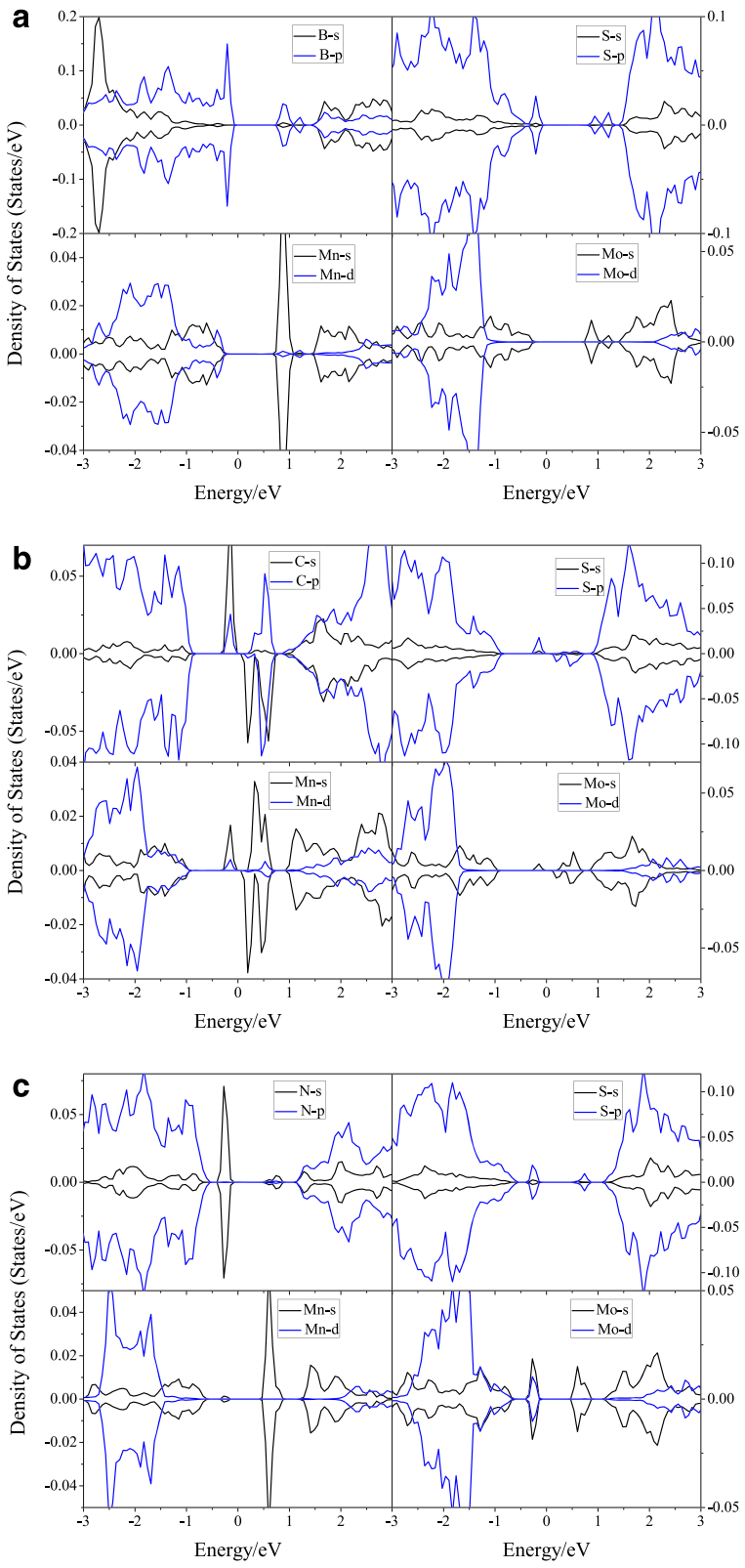

Figure 3 P-DOS of $Mo_{15}MnBS_{31}$ (a), $Mo_{15}MnCS_{31}$ (b), and $Mo_{15}MnNS_{31}$ (c).

structures are shown in Figure 4; Mn-B and Mn-N co-doping make the energy bandgap become smaller than before, where the bandgaps are 1.03 and 0.81 eV, respectively. And the $Mo_{15}MnNS_{31}$ transforms into an indirect semiconductor. Unsurprisingly, the Mn-B (N) co-doping cannot transform the spin state of the material, which makes the system stay in a nonmagnetic state. It is due to the effective charge compensation between Mn or B (N) atoms. But the Mn-C co-doped system reflects spin polarization and the magnetic moment is 0.87 μB. The generation of the magnetic moment is mainly because Mn provides one more electron than the Mo atom; when C substitutes for the S atom, it needs more electrons to make the 2p orbit saturated. In Figure 4c,d, a series of impurity bands appear around the Fermi level which results in the reinforcement of the light absorption and expands the absorbed region. These strong local lines come from the orbital hybridization between C-2 s, C-2p and Mn-3d, Mn-4 s, Mo-5 s, which provide more electronic states in energy space per unit. For Figure 4a,b, we can clearly see that the Fermi level shifts down, which means that $Mo_{15}MnBS_{31}$ can provide amounts of vacancies. Figure 4e,f indicates that the Fermi level shifts up and $Mo_{15}MnNS_{31}$ provides plenty of electrons. All of the co-doped systems gain different abilities of electronic transition between the top of the valence band (TVB) and the bottom of the conduction band (BCB). By comparing the energy band structures, the Mn-C co-doped MoS_2 monolayer has a higher spin polarization. Orbital hybridization makes the valence exclusion effect stronger in $Mo_{15}MnCS_{31}$. The narrowness of the bandgap indicates that the absorbed region of this semiconductor becomes larger. This result is well consistent with the density of state before.

Optical property

The optical properties of $Mo_{15}MnBS_{31}$, $Mo_{15}MnCS_{31}$, and $Mo_{15}MnNS_{31}$ all reflect the redshift phenomenon which leads to the MoS_2 monolayer absorbing more infrared light. The optical property of the primitive state well agrees with studies before [37,38].

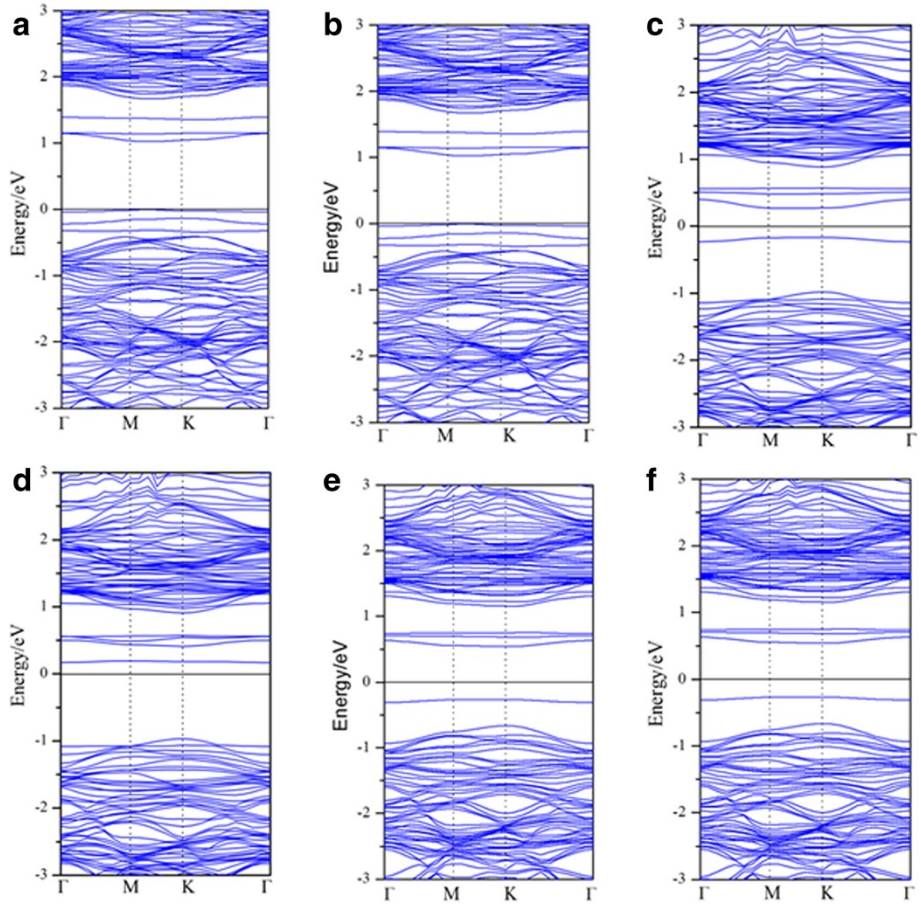

Figure 4 The energy band of the doped structures. (a, b) Mn-B co-doped MoS_2 monolayer, **(c, d)** Mn-C co-doped MoS_2 monolayer, **(e, f)** Mn-N co-doped MoS_2 monolayer. The former of the pattern in pairs shows the energy band of spin-up, and the latter shows the band structure of spin-down.

In Figure 5a, $Mo_{15}MnBS_{31}$, $Mo_{15}MnCS_{31}$, and $Mo_{15}MnNS_{31}$ all emerge as a series of peaks between 0 and 2 eV because of the electronic transition between B-2p and Mn-4 s; C-2 s, C-2p and Mn-3d, Mn-4 s; and N-2 s and Mn-4 s, Mo-5 s near the Fermi level, respectively. In $Mo_{15}MnBS_{31}$, $Mo_{15}MnCS_{31}$, and $Mo_{15}MnNS_{31}$, the peaks of the dielectric function all reflect the redshift phenomenon in which the value of the peaks in the high-energy region becomes gentle and small and the whole tendency gains no more changes. However, the peak of the dielectric function for $Mo_{15}MnBS_{31}$ is the largest in the low-energy area. It illustrates that the electronic transition between B-2p and Mn-4 s is active during this region.

In Figure 5b, the absorption edge of the pure molybdenum disulfide monolayer is 0.8 eV, corresponding to the electrons which transfer from the conduction band to the valence band partially, which is in very good agreement with the experimental value [7]. The co-doped structures all reflect the redshift phenomenon, and the absorption edges of the Mn-B, Mn-C, and Mn-N systems become 0.45, 0.5, and 0 eV, respectively. And the value of absorption peaks decreased simultaneously. The redshift phenomenon shows us that the co-doped systems have better optical gas sensing property. Although the number of absorption peaks decreased, the energy range increased, which indicates that the wavelength range for the absorption became wider. In the high-energy region, the absorption of $Mo_{15}MnBS_{31}$, $Mo_{15}MnCS_{31}$, and $Mo_{15}MnNS_{31}$ is so little such that the MoS_2 monolayer has high transmittance in the visible light region under these circumstances. These findings indicate that the pure MoS_2 is more suitable to make a near-ultraviolet (6.0 ~ 6.5, 6.8 ~ 7.0, and 8.5 ~ 9.5 eV) photodetector than the MoS_2 monolayer co-doped with Mo-B (C, N). But $Mo_{15}MnCS_{31}$ is the most suitable to make a near-ultraviolet (3.3 ~ 5.8 eV) photodetector. The Mn-B co-doped MoS_2 monolayer is more suitable to make an infrared photodetector.

Figure 5c,d shows us the reflectivity and refractivity of the MoS_2 monolayer. $Mo_{15}MnBS_{31}$, $Mo_{15}MnCS_{31}$, and $Mo_{15}MnNS_{31}$ all produce a series of peaks in the low-energy area and reflect the redshift phenomenon. These peaks are mainly due to the electronic transition of B-2p and Mn-4 s; C-2 s and Mn-3d, Mn-4 s; and N-2 s and Mn-4 s, respectively. Due to the active electronic transition between B-2p and Mn-4 s as well as the symmetry breaking induced by the Mn-B dopant, $Mo_{15}MnBS_{31}$ owns a maximum peak. On the contrary, in the infrared light region, $Mo_{16}S_{32}$ gets the minimum reflectivity. Hence, $Mo_{16}S_{32}$ obtains high transmittance in the infrared light region. The variation tendency of the primitive MoS_2 monolayer in reflectivity is consistent with what Newaz has done [9].

Conclusions

According to our calculation, the electronic structure and optical properties of Mn and B, C, N co-doped MoS_2 monolayers have been investigated through first-principles. As is shown, the MoS_2 monolayer co-doped with Mn-C reflects magnetism and the magnetic moment is 0.87 μB. It is due to the Mn providing one more

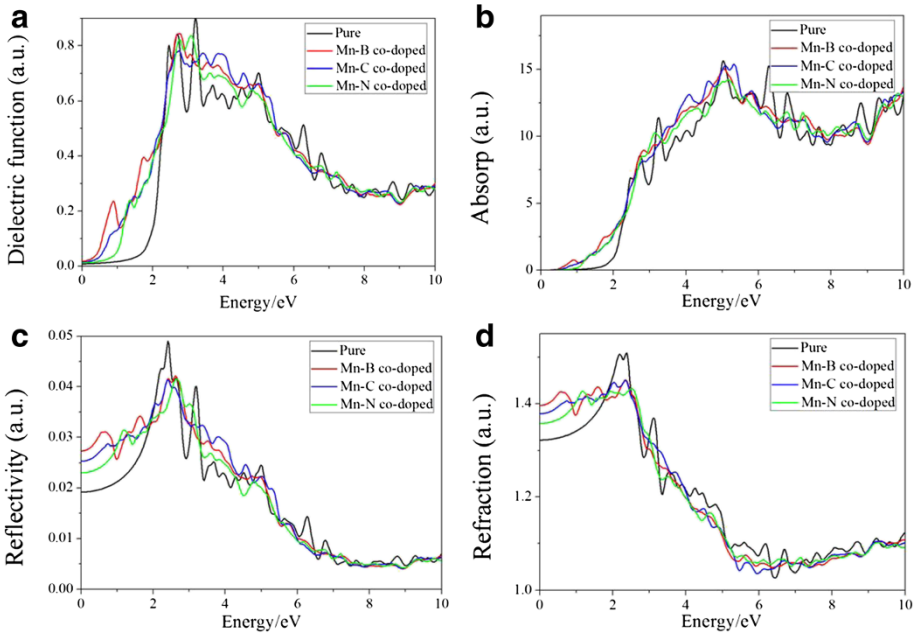

Figure 5 The optical properties of $Mo_{16}S_{32}$ (black line), $Mo_{15}MnBS_{31}$ (red line), $Mo_{15}MnCS_{31}$ (blue line), and $Mo_{15}MnNS_{31}$ (green line). **(a)** Dielectric function, **(b)** absorption, **(c)** reflectivity, and **(d)** refractivity.

electron than the Mo atom; when C substitutes for the S atom, it needs more electrons to make the 2p orbit saturated. However, the co-doped systems with Mn and B (N) atoms exhibit semiconducting behavior with bandgaps smaller than those of the corresponding pristine state because of the effective charge compensation between Mn and B (N) atoms. And the energy bandgaps are 1.03 and 0.81 eV, respectively. Mn-B (C, N) co-doping all make the optical absorption edges generate the redshift phenomenon for the MoS_2 monolayer, which results in the enhancement of the MoS_2 monolayer absorbing infrared light. The absorption edge of the pure molybdenum disulfide monolayer is 0.8 eV, where the absorption edges of Mn-B, Mn-C, and Mn-N co-doped systems become 0.45, 0.5, and 0 eV, respectively. $Mo_{15}MnCS_{31}$ is easier to achieve in the experiments than other structures. As a potential material, it is necessary to realize the tunable bandgap in the MoS_2 monolayer by surface adsorption. Furthermore, our research will progress towards quantum transport simulation and tunneling transistors like silicene [39,40].

Competing interests
The authors declare that they have no competing interests.

Authors' contributions
P-JW and C-WZ conceived the idea and designed the calculated model. W-BX carried out the electronic structure calculations and data analysis. PL, FL, and B-JH performed the analysis method of optical properties. All authors read and approved the final manuscript.

Acknowledgements
This work was supported by the National Natural Science Foundation of China (Grant Nos. 61172028, 11274143, and 11304121) and the Natural Science Foundation of Shandong Province (Grant No. ZR2010EL017).

Received: 15 July 2014 Accepted: 9 September 2014
Published: 6 October 2014

References
1. Friend H, Yoffe A: **Layer compounds.** *Ann Rev Mater Sci* 1973, **3:**147–170.
2. Levy F: **Intercalated layered materials.** *Physics and Chem Mater with A* 1979, **6:**99–100.
3. Han SW, Kwon H, Kim SK: **Band-gap transition induced by interlayer van der Waals interaction in MoS_2.** *Phys Rev B* 2011, **84:**045409.
4. Lebegue S, Eriksson O: **Electronic structure of two-dimensional crystals from *ab initio* theory.** *Phys Rev B* 2009, **79**(11):115409.
5. Li T, Galli G: **Electronic properties of MoS_2 nanoparticles.** *J Phys Chem C* 2007, **111**(44):16195–16196.
6. Ataca C, Sahin H, Akturk E: **Mechanical and electronic properties of MoS_2 nanoribbons and their defects.** *J Phys Chem C* 2011, **115**(10):3934–3941.
7. Mak KF, Lee C, Shan J, Heinx TF: **Atomically thin MoS_2: a new direct-gap semiconductor.** *Phys Rev Lett* 2010, **105:**136805.
8. Splendiani A, Sun L, Zhang Y: **Emerging photoluminescence in monolayer MoS_2.** *Nano Lett* 2010, **10**(4):1271–1275.
9. Newaz AKM, Prasai D, Ziegler JI: **Electrical control of optical properties of monolayer MoS_2.** *Solid State Commun* 2013, **155:**49–52.
10. Hwang H, Kim H, Cho J: **MoS_2 nanoplates consisting of disordered graphene-like layers for high rate lithium battery anode materials.** *Nano Lett* 2011, **11:**4826–4830.
11. Bertolazzi S, Brivio J, Kis A: **Stretching and breaking of ultrathin MoS_2.** *ACS Nano* 2011, **5:**9703–9709.
12. Eda G, Yamaguchi H, Voiry D, Fujita T, Chen M, Chhowalla M: **Photoluminescence from chemically exfoliated MoS_2.** *Nano Lett* 2012, **11:**5111–5116.
13. Cao T, Wang G, Han W: **Valley-selective circular dichroism of monolayer molybdenum disulphide.** *Nat Commun* 2012, **3:**887–892.
14. Mak K, He K, Shan J, Heinz TF: **Control of valley polarization in monolayer MoS_2 by optical helicity.** *Nat Nanotechnol* 2012, **7:**494–498.
15. Cheng YC, Zhu ZY, Mi WB: **Prediction of two-dimensional diluted magnetic semiconductors: doped monolayer MoS_2 systems.** *Phys Rev B* 2013, **87:**100401.
16. Fan XB, Liu F, Yao SY: **Preparation of MoS_2 nanocatalyst and its application in hydrodesulfurization.** *J Cata* 2012, **33:**1027–1031.
17. Pollack SS, Makovsky LE, Brown FR: **Identification by X-ray diffraction of MoS_2 in used $CoMoAl_2O_3$ desulfurization catalysts.** *J Cata* 1979, **59**(3):452–459.
18. Kam KK, Parkinson B: **Detailed photocurrent spectroscopy of the semiconducting group VIB transition metal dichalcogenides.** *J Chem Phys* 1982, **86**(4):463–467.
19. Young PA: **Lattice parameter measurements on molybdenum disulphide.** *J Phys D Appl Phys* 1968, **1**(7):936.
20. Böker T, Severin R, Müller A: **Band structures of MoS_2, $MoSe_2$ and a-$MoTe_2$: angle-resolved photoelectron spectroscopy in the constant-final-state mode and *ab initio* calculations.** *Phys Rev B* 2001, **64:**235–305.
21. Kim C, Kelty S: **Near-edge electronic structure in NbS_2.** *J Chem Phys* 2005, **123:**244705.
22. Fang CM, Ettema ARHF, Haas C: **Electronic structure of the misfit-layer compound $(SnS)_{1.17}NbS_2$ deduced from band-structure calculations and photoelectron spectra.** *Phys Rev B* 1995, **52:**2336.
23. Novoselov KS, Jiang D, Schedin F, Booth TJ: **Two-dimensional atomic crystals.** *Proc Nat Acad Sci USA* 2005, **102:**10451–10453.
24. Ayari A, Cobas E, Ogundadegbe O: **Realization and electrical characterization of ultrathin crystals of layered transition-metal dichalcogenides.** *J Appl Phys* 2007, **101:**014507.
25. Yue Q, Chang S, Qin S: **Functionalization of monolayer MoS_2 by substitutional doping: a first-principles study.** *Phys Lett A* 2013, **377**(19):1362–1367.
26. Ramasubramaniam A, Naveh D: **Mn-doped monolayer MoS_2: an atomically thin dilute magnetic semiconductor.** *Phys Rev B* 2013, **87**(19):195201.
27. Sun QC, Mazumdar D, Yadgarov L: **Spectroscopic determination of phonon lifetimes in rhenium-doped MoS_2 nanoparticles.** *Nano Letter* 2013, **13**(6):2803–2808.
28. Blaha P, Schwarz K, Madsen GKH, Kvasnicka D: **WIEN2k, an augmented plane wave +local orbitals program for calculating crystal properties.** 2001, 165–168.
29. Perdew JP, Burke K, Ernzerhof M: **Generalized gradient approximation made simple.** *Phys Rev Lett* 1996, **77**(18):3865.
30. Coehoorn R, Haas C, Dijkstra J: **Electronic structure of $MoSe_2$, MoS_2, and WSe_2. I. Band-structure calculations and photoelectron spectroscopy.** *Phys Rev B* 1987, **35:**61–95.
31. Kobayashi K, Yamauchi J: **Electronic structure and scanning-tunneling-microscopy image of molybdenum dichalcogenide surfaces.** *Phys Rev B* 1995, **51**(23):17085.
32. Ye LH, Freeman AJ, Delley B: **Half-metallic ferromagnetism in Cu-doped ZnO: density functional calculations.** *Phys Rev B* 2006, **73:**033203.
33. Xiao WZ, Wang LL, Xu L: **First-principles study of magnetic properties in Ag-doped SnO_2.** *Phys Status Solidi B* 2011, **248**(8):1961–1966.
34. Pan H, Zhang YW: **Edge-dependent structural, electronic and magnetic properties of MoS_2 nanoribbons.** *J Mate Chem* 2012, **22**(15):7280–7290.
35. Rahman G, Morbec JM: **Intrinsic magnetism in nanosheets of SnO_2: a first-principles study.** *J Magnetism Magn Mater* 2013, **328:**104–108.
36. Ivanovskaya VV, Zobelli A, Gloter A: ***Ab initio* study of bilateral doping within the MoS_2-NbS_2 system.** *Phys Rev B* 2008, **78:**134104–134117.
37. Singh N, Jabbour G: **Optical and photocatalytic properties of two-dimensional MoS_2.** *J Euro Phys B* 2012, **85**(11):1–4.
38. Shi HL, Pan H: **Quasiparticle band structures and optical properties of strained monolayer MoS_2 and WS_2.** *Phys Rev B* 2013, **87**(15):155304.
39. Quhe R, Fei R, Liu Q: **Tunable and sizable band gap in silicene by surface adsorption.** *Sci Rep* 2012, **2:**853–858.
40. Ni Z, Zhong H, Jiang X: **Tunable band gap and doping type in silicene by surface adsorption: towards tunneling transistors.** *Nanoscale* 2014, **6**(13):7609–7618.

doi:10.1186/1556-276X-9-554
Cite this article as: Xu *et al.*: The electronic structure and optical properties of Mn and B, C, N co-doped MoS_2 monolayers. *Nanoscale Research Letters* 2014 **9**:554.